Energy, Volume 321, April 2025, Article number 135358
10.1016/j.energy.2025.135358

An advanced performance-based method for soft and abrupt fault diagnosis of industrial gas turbines

Yu-Zhi Chen[1], Wei-Gang Zhang[2], Elias Tsoutsanis[3,*], Junjie Zhao[4], Ivan C.K. Tam[5], Lin-Feng Gou[6]
[*] Corresponding author (elias.tsoutsanis@tii.ae)

ABSTRACT

Integrating gas turbines with intermittent renewable energy must operate for prolonged periods under transient conditions. Existing research on fault diagnosis in such systems has concentrated on the primary rotating components in steady-state conditions. There is a growing interest in investigating the interplay between shaft bearing failure and performance metrics, as well as fault identification under transient conditions. This study aims to identify faults not only in the main rotating components but also in the shaft bearings under transient conditions. Firstly, the performance model and fault propagation model of gas turbines are established, and the influence of bearing fault on the whole engine performance is analysed. Then, the fault diagnosis method is determined and the dynamic effects are compensated in fault identification at each time interval. Finally, the steady-state and transient fault diagnosis are carried out, considering the constant and sudden faults for the main rotating components and bearings. The average run time and maximum error at steady state conditions are 0.1064 s and 0.0086%, respectively. For the proposed dynamic effects compensation method, the average computation time and peak error for each time instant during the transient manoeuvre are 0.1152 s and 0.0143%, respectively, clearly superior to the benchmark method. These results demonstrate that the proposed method can diagnose accurately the fault of the main rotating components and shaft bearings under transient conditions. Therefore, the findings mark an advancement in

[1] School of Power and Energy, Northwestern Polytechnical University, Xi'an 710129, China
[2] School of Power and Energy, Northwestern Polytechnical University, Xi'an 710129, China
[3] Propulsion and Space Research Center, Technology Innovation Institute, Masdar City, PO Box: 9639, Abu Dhabi, United Arab Emirates
[4] School of Aerospace, Transport and Manufacturing, Cranfield University, Bedfordshire MK43 0AL, UK
[5] Faculty of Science, Agriculture & Engineering, Newcastle University, Newcastle upon Tyne NE1 7RU, UK
[6] School of Power and Energy, Northwestern Polytechnical University, Xi'an 710129, China

Published by Elsevier. This is the Author Accepted Manuscript issued with: Creative Commons Attribution License (CC:BY 4.0).
The final published version (version of record) is available online at DOI:10.1016/j.energy.2025.135358. Please refer to any applicable publisher terms of use.

real-time fault diagnostic techniques, ultimately enhancing engine availability while upholding secure and affordable energy production.

Key Words: Gas Turbine Deterioration; Continuous Gas Path Analysis; Real-time; Main Rotating Components Fault; Shaft Bearing Fault.

Nomenclature

A = Heat transfer area $[m^2]$

CW = Compressor work $[W]$

$EFLH$ = Equivalent full load hour $[W]$

EL = External load by power offtake $[W]$

HPC = High-pressure compressor

HPT = High-pressure turbine

$HPSB$ = High-pressure shaft bearing

I = Shaft inertia $[kg \cdot m^2]$

ICM = Influence coefficient matrix

$LPSB$ = Low-pressure shaft bearing

LPT = Low-pressure turbine

m = Decay rate of degradation factor

n = Exponential time-scaling coefficient

N = Shaft rotational speed $[rpm]$

$\dot{N}$ = Shaft rotational acceleration $[rad/s^2]$

PC = Performance characteristic

PS = Power setting $[MW]$

Q = Heat transfer between gas and metal $[W]$

RE = Relative error

$RMSE$ = Root mean square error

SP = Surplus power $[W]$

T = Temperature $[Kelvin]$

TW = Turbine work $[W]$

U = Heat transfer coefficient $[W/(m^2 \cdot K)]$

W = Mass flow rate $[kg/s]$

X = Degradation factor

Y = Power-setting parameters

Z = Measurements

Greek Letters

η = Efficiency

ρ = Density $[kg/m^3]$

τ = Time constant $[s]$

Subscripts

d = Degraded condition

g = Gas

GT = Gas turbine

h = Healthy condition

HP = High pressure

HPSB = High-pressure shaft bearing

HPT = High-pressure turbine

LPSB = Low-pressure shaft bearing

LPT = Low-pressure turbine

in = Input

LP = Low pressure

m = Metal

out = Output

P = Predicted

1. Introduction

Fault diagnosis for condition-based maintenance is receiving increased attention across an expanding number of disciplines [1,2]. Gas path analysis (GPA), as a means of improving the reliability and safety of gas turbines, has been an established practice since 1969 [3], but recently it has attracted considerable critical attention [4]. Recent developments in the field of novel power systems have led to a great interest in integrating gas turbines with renewable energy sources, for example, wind and solar power, to achieve carbon neutrality [5,6]. However, renewable energy has the characteristics of intermittency, randomness, and fluctuations, which can affect grid stability [7]. Therefore, the gas turbines in such systems will spend prolonged periods operating under transient conditions to achieve grid control [8]. Correspondingly, there is increasing interest in GPA under transient conditions, especially for sudden failure during dynamic operation.

GPA has been studied extensively about gas turbines working under steady-state conditions. Tsoutsanis and Meskin [9] combined fault diagnosis with window-based regression for performance prognosis in 2017. Li and Ying [10] introduced an advanced GPA method for sensor, compressor, burner, and turbine deterioration when gas turbine power shifts with power demand. Hanachi et al. [11] analysed a hybrid fault diagnosis method that combines the fault parameter with fault propagation to deal with multiple component degradation simultaneously. Montazeri and Yazdani [12] studied the classification of faults in gas turbines based on an Interval Type-2 Fuzzy Logic System. Chen and his co-workers developed a novel gas path analysis technique to increase computing validity and speed in 2021 [13]. Mantelli et al. [14] reported a diagnostic approach based on a Bayesian belief network for combined solid oxide fuel cells and gas turbine power plants. Zhao et al. [15] conducted a hierarchical diagnostic approach for large bypass ratio turbofan engines to overcome the lack of physical insight of traditional machine learning-based methods.

The last few years have seen a surge of research directed at using GPA to analyse the transient behaviour of gas turbine engines. Sampath et al. [16] conducted shaft bearing fault diagnosis based on gas path measurements under dynamic conditions. Li [17] suggested a GPA method based on accumulated deviation during a transient manoeuvre.

Mousavi [18] used adaptive methods for fault detection and isolation in heavy-duty industrial gas turbines. Amirkhani et al. [19] introduced a diagnostic method based on a series-parallel NARX model for fault detection in gas turbines. Using a surrogate model, Cheng et al. [18] investigated faults developed in a dual-shaft industrial gas turbine under dynamic conditions and proposed a real-time GPA method for turbofan engines operating in steady-state and dynamic conditions. Ying and Li [20] examined a steady-state approximation fault diagnosis scheme for heavy-duty industrial gas turbines with large inertia under transient conditions. However, limited studies seek to identify shaft bearing sudden failure by GPA. Fig. 1 presents the inter-shaft bearing fault, which will deteriorate the mechanical efficiency of the engine shaft [21]. Consequently, shaft bearing faults will impact component matching, deteriorate engine performance, and delay the dynamic response of the gas turbine.



Fig. 1 Faults in the inter-shaft bearing [21].

While GPA for major rotating components of gas turbines is a sound field, publications on GPA for shaft bearing faults are limited. To the best of the authors' knowledge, no previous study has systematically investigated the effect of the health of shaft bearings on engine performance and fault diagnosis. In addition, the GPA for both major rotating components and shaft bearings has not been comprehensively studied under both steady-state and transient conditions. Notably, fault diagnosis of shaft bearing sudden failure at dynamic conditions has not been investigated. Therefore, it is necessary to carry on continuous fault diagnosis for major rotating components and shaft bearings, especially sudden failure during transient status. One of the main obstacles of GPA under transient conditions is the dynamic effects of the engine working under unstable conditions. In that case, the gas path measurements cannot be used independently for fault diagnosis and the measurements should be considered as a time series.

This study will help bridge this gap in the literature and address the dynamic effects for achieving a reliable and accurate fault diagnosis of gas turbines. The novel contribution of this study is to proposed a GPA method to diagnose the main rotational components and shaft bearing fault under dynamic conditions simultaneously, even with a sudden failure. Furthermore, the suggested approach is also compared empirically with the state-of-the-art method [20] in order to demonstrate the noteworthy benefits of employing dynamic effect compensation. This study also offers an

innovative perspective on the effect of shaft bearing faults on engine performance and fault diagnosis. The study offers important insights into implementing a hydrogen-fuelled gas turbine for power generation. The novel contributions of this paper are as follows:

1) A study has been carried out to assess the detrimental effects of shaft bearing failure on engine performance and fault identification.
2) A continuous method for diagnosing faults in industrial gas turbines is proposed using dynamic effect compensation under transient conditions.
3) The health status of three rotating components and shaft bearings can be identified simultaneously with high precision in real-time under both steady-state and transient conditions, even in the case of sudden failure.
4) To date, no attempts have been made to diagnose the sudden failure of a shaft bearing using GPA under transient conditions. This study will extend the use of GPA to the sudden failure of shaft bearings under transient conditions.

This paper begins by summarising the recent development of the use of GPA and the restriction of the current study. The second section presents the methodology employed, and the third section examines the engine model developed for transient and steady-state conditions. The fourth section demonstrates the adverse effects of shaft bearing deterioration and validates the proposed method with test cases. The major deliverables and significant findings are concluded in the final section.

2. Methodology

2.1 Assumptions

In this study, several assumptions were made when verifying the effectiveness and capabilities of the methods used.

- Extensive studies exist in the open literature to deal with measurement noise/bias [22,23]. Hence, this study will not cover sensor-related problems to provide a clear view of diagnostic precision without prejudice.
- The efficiency, flow capacity, and pressure ratio degradation factor define the fault level of the main rotational components, assuming that the relative deviations of flow capacity and pressure ratio are the same [24].
- The mechanical efficiency degradation factors represent the shaft bearing fault level [17].

- All main rotational components and shaft bearings are assumed to deteriorate with faults that develop with time following an exponential law [25]. In addition, all components of concern could suffer from a sudden failure simultaneously at dynamic conditions to test the robustness of the method proposed.

2.2 Gas Turbine Performance and Degradation Modelling

2.2.1 Engine Configuration

As shown in Fig. 2, the engine being considered is a dual-shaft land-based gas turbine similar to the LM2500+ designed by General Electric [26]. It includes a HPC, a burner, a HPT followed by the LPT co-shafted with the electric generator. The HP and LP shafts are supported by the $HPSB$ and $LPSB$, respectively. Table 1 lists the available engine gas path measurements.

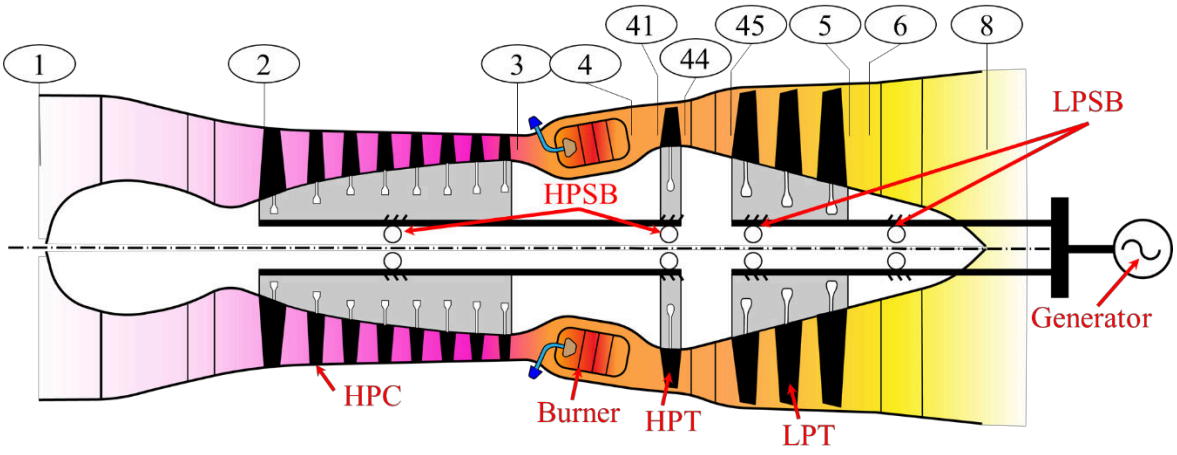


Fig. 2 Cutaway section of gas turbine in concern.

Table 1 Available engine gas path measurements [27].

No	Measurement	Symbol
1	Engine inlet pressure	P_1
2	Engine inlet temperature	T_1
3	Inlet pressure to *HPC*	P_2
4	Inlet temperature to *HPC*	T_2
5	Exit pressure from *HPC*	P_3
6	Exit temperature from *HPC*	T_3
7	Inlet pressure to *LPT*	P_{45}
8	Inlet temperature to *LPT*	T_{45}
9	Exit pressure from *LPT*	P_5
10	exit temperature from *LPT*	T_5
11	Rotational speed of *LP* shaft	N_{LP}

12	Rotational speed of *HP* shaft	N_{HP}
13	Flow rate of fuel to burner	W_{Fuel}

2.2.2 Engine Performance Modelling

A component-level model has been developed and validated by Chen and co-workers, first for an industrial triple-shaft gas turbine fuelled by natural gas [13], and then for a dual-shaft turbofan engine powered by hydrogen [28]. The core of both models is *TurboWorkX*, which is a modular gas turbine performance simulation software. This study will use the components of *TurboWorkX* to build a model of a dual-shaft industrial engine fuelled by hydrogen. For the detailed theory of each component refer to Kurzke and Halliwell [29].

2.2.3 Definition of Degradation

In this study, the degradation of major rotational components and shaft bearings will be considered simultaneously. Extensive research has shown that, typically, the overall performance of an engine is determined by the performance characteristics (PC) of the individual subcomponents [30,31]. Accordingly, the degradation factor (X) of each performance characteristic of any particular component can be defined by Eq. **(1)** to quantify the deviation of the degraded state from the healthy [32,33].

$$X = \frac{PC_d}{PC_h} \tag{1}$$

where the subscripts "d" and "h" denote degraded and healthy conditions, respectively. A value of 1 is taken to mean the engine is in a healthy condition [8,34].

Table 2 Degradation factors of the given gas turbine.

Component	Symbol		Degradation Factor	Health Status I	Health Status II [35]
HPC	X_{HPC}	$X_{HPC,E}$	Efficiency factor, *HPC*	-4.70 %	-9.40 %
		$X_{HPC,F}$	Flow capacity factor, *HPC*	-7.03 %	-14.06 %
HPT	X_{HPT}	$X_{HPT,E}$	Efficiency factor, *HPT*	-1.905 %	-3.81 %
		$X_{HPT,F}$	Flow capacity factor, *HPT*	+1.285 %	+2.57 %
LPT	X_{LPT}	$X_{LPT,E}$	Efficiency factor, *LPT*	-0.539 %	-1.078 %
		$X_{LPT,F}$	Flow capacity factor, LPT	+0.2113 %	+0.4226 %
$HPSB$	X_{HPSB}		Mechanical efficiency factor HP shaft	-3%	-6%
$LPSB$	X_{LPSB}		Mechanical efficiency factor, LP shaft	-1.5%	-3%

A summary of the degradation factors and health status relevant to the gas turbine is presented in Table 2. 'Health State I' refers to a dual-shaft industrial gas turbine that has completed 25,000 equivalent full load hours (EFLHs) of operation, and for 'Health Status II', the degradation is twice as severe as in 'Health Status I'. The shift from 'Health Status I' to 'Health Status II' represents a sudden engine failure.

2.2.4 Fault Propagation

As stated above, it is assumed that the 'Health Status I' in Table 2 corresponds to 25,000 EFLHs, which means that an overhaul for the gas turbine is required. Fault propagation is defined in Eq. **(2)**, which represents the progressive development of a component fault with $EFLH$.

$$|\Delta X| \cdot X = |PC_d - PC_h| = 1 - exp(m \cdot EFLH^n) \quad \textbf{(2)}$$

where m is the decay rate of the degradation factor, and n is the exponential time-scaling factor. In Appendix A, Table A- 1 summarises m and n for each degradation factor.

2.3 Dynamic Effect Compensation

When an engine works under transient conditions, no component of the engine is operating under thermodynamic equilibrium. For example, under acceleration, the work done by the turbine might be greater than the work done by the co-shaft compressor due to power offtake, and vice versa. Hence, the gas path measurements monitored separately at each time instant cannot be used for GPA and would not give valid feedback on the health of the engine. In such an arrangement, the dynamic effect should be included to allow the diagnostic system to conduct fault diagnosis at each instant, especially under transient conditions.

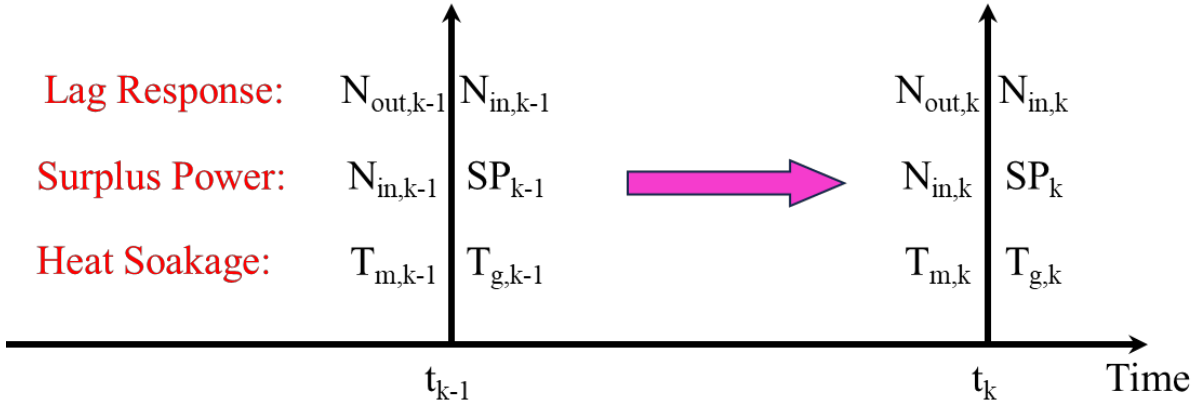


Fig. 3 Dynamic effect compensation timing diagram.

This study considers three typical dynamic effects: the lag response of the speed sensor, rotor dynamics, and heat soakage. Fig. 3 demonstrates the timing diagram of dynamic effect compensation.

The measured rotor speed with delay must be updated to find the actual rotational speed. In addition, the surplus power (SP) must be obtained from the rotational speed at the adjacent time step. Finally, the engine metal temperature from the previous step will be used to calculate the gas and metal temperatures at the current step after heat transfer. If the dynamic effects are ignored, the approach is known as the steady-state approximation method [36]. It is worth noting that if the dynamic effects are not appropriately considered in the diagnosis system, the diagnosed results will be in error and may potentially activate false alarms, which will significantly affect the credibility of the engine operation and maintenance teams. However, the regression technique is limited to large thermo-mechanical inertia applications such as heavy-duty industrial gas turbines. A more detailed explanation of the dynamic compensation effect is as follows:

2.3.1 Lag Response of Speed Sensor

Under transient conditions, the shaft rotational speed, as measured by the sensor, is likely to lag the actual speed. If the rotational speed used in the engine model is not the actual speed, an incorrect shaft speed value will be used to read the compressor and turbine maps. The negative effect of lag response is addressed through first-order lag theory defined by Eq. **(3)** [37,38].

$$\frac{N_{out}(s)}{N_{in}(s)} = \frac{1}{1 + s \cdot \tau} \tag{3}$$

where τ is the time constant, $N_{in}(s)$ represent the actual shaft speed and $N_{out}(s)$ the shaft speed measured by a sensor with delay.

2.3.2 Rotor Dynamics

As mentioned above, the expansion work in the turbine is not equal to the power needed during a transient manoeuvre [39]. In order to meet the power required for each shaft, it is necessary to quantify the surplus power (SP) for every shaft and reconstitute the shaft power identity equation. Under dynamic conditions, the acceleration and deceleration of shafts can be expressed using Eq. **(4)** [40,41], which is related to the shaft acceleration rate ($\dot{N}$), shaft rotational speed (N) and shaft moment of inertia (I).

$$\dot{N} = \frac{60^2}{4 \cdot \pi^2} \cdot \frac{SP}{N \cdot I} \tag{4}$$

Then, the SP could be obtained based on moving and changing the terms based on Eq. **(4)** as follows. Clearly, when $\dot{N}$ is available, the SP at each time instant can be found. Under steady-state conditions this will be equal to zero as the shaft acceleration is none.

$$SP = \frac{4 \cdot \pi^2}{3600} \cdot \dot{N} \cdot N \cdot I \tag{5}$$

$\dot{N}$ can be obtained from Eq. **(6)** [42,43], which is a more advanced control parameter when compared to the traditional gas turbine speed control,

$$\dot{N} = \frac{N(t) - N(t - \Delta t)}{\Delta t} \tag{6}$$

where Δt is the time step between two adjacent moments.

The identical power equations for the HP shaft could be determined by Eq. **(7)** [44,45]. It is worth noting that the equality of two equations is established for both steady-state and transient status,

$$TW_{HPT} = SP_{HP} + CW + EL \tag{7}$$

where TW_{HPT} is work done by the HP turbine, CW is the work needed for compressing air in the co-shaft compressor, and EL is external load by power offtake.

Regarding the LP shafts, the identical power equations could be found in Eq. **(8)**.

$$TW_{LPT} = SP_{LP} + PS \tag{8}$$

where TW_{LPT} is low pressure turbine work, and PS is the power setting in the co-shaft generator.

2.3.3 Heat Soakage

It is known that the metal and gas temperature will be in thermal equilibrium under steady-state conditions. However, the thermal inertia of the metal in the engine will delay the heat balance under dynamic conditions, especially under a reslam manoeuvre. Fig. 4 depicts the transient working line of the compressor under hot reslam, which occurs when the engine runs at a high power setting for a while before abruptly decreasing power and accelerating back up to a high power setting [46]. Note that the compressor transient working line with reslam is closer to the surge margin than normal acceleration. Attention must be paid to out-of-norm conditions because during transient state manoeuvres and novel power cycles, the gas will need to operate in such a manner to maintain grid stability. It is reported that the engine exhaust gas temperature will be significantly delayed due to heat soakage [47].

Therefore, if the heat soakage is ignored, the relative error of exhaust gas temperature and other gas path measurements will propagate to the diagnostic results. It is important to note that heat soakage will raise the average and maximum gas path analysis error by 1.1% and 7%, respectively, with a harsh acceleration [48].

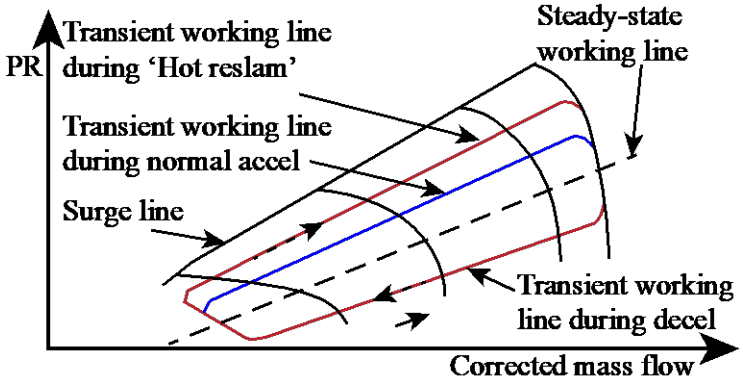


Fig. 4 Compressor transient working line under hot reslam [46].

The proposed method for fault diagnosis considers heat soakage for various operating conditions. The heat soakage is calculated using Eq. **(9)**, which includes a delay with exponential form [47]. For a more detailed description of the process, refer to [48].

$$Q = A \cdot U \cdot (T_g - T_m) \cdot (e^{-\Delta t/\tau} - 1) \tag{9}$$

where Q is heat transfer between gas and metal, A is area of heat transfer, U is coefficient of heat transfer, T_g is gas temperature, T_m is the engine metal temperature, and τ is the time constant.

2.4 Diagnosis Scheme

Although the health condition of an engine cannot be measured directly, the effect of the deterioration of each component will be reflected in the measured parameters. The relation between degradation factors (X), power-setting parameters (Y), and engine measurements (Z) can be defined by Eq. **(10)**,

$$Z = ICM(X, Y) \tag{10}$$

where ICM is the influence coefficient matrix.

Fig. 5 shows the layout of the diagnostic schematic used in this study. The value of X could be obtained by an iteration solver, which minimises the difference between predicted and actual measurements. The Newton-Raphson [51] method is adopted in this study for engine performance simulation and GPA.

$RMSE$ was selected to evaluate the convergence of fault diagnosis within the pre-set threshold (1E-5) using Eq. **(11)** [49,50].

$$RMSE = \sqrt{\sum_{i=1} \frac{(Z_{P,i} - Z_{A,i})^2}{k}} \tag{11}$$

where $Z_{P,i}$ is predicted parameter of ith measurement, $Z_{A,i}$ is the ith measurement of the actual parameter, and k is the total number of measurements.

The relative error (RE) of the diagnosis is defined by Eq. **(12)**:

$$RE_j = 100\% \cdot \frac{\left|X_{P,j} - X_{A,j}\right|}{X_{A,j}} \tag{12}$$

where $X_{P,j}$ is predicted value of jth degradation factor, $X_{A,j}$ is the actual value of jth degradation factor.

The investigation process is shown in Fig. 6 for the entire range of operating conditions. The fuel flow rate is the "Handle" parameter of the gas turbine engine. Table 2 summarises the degradation factors of concern, which are blocked in purple in Fig. 6. The direct gas path measurements like ambient temperature (T_1) and pressure (P_1) and indirect gas path measurements such as surplus power (SP) and metal temperature at combustor outlet ($T_{4,M}$) are presented in green blocks. The components of the gas turbine model are presented in the red blocks.

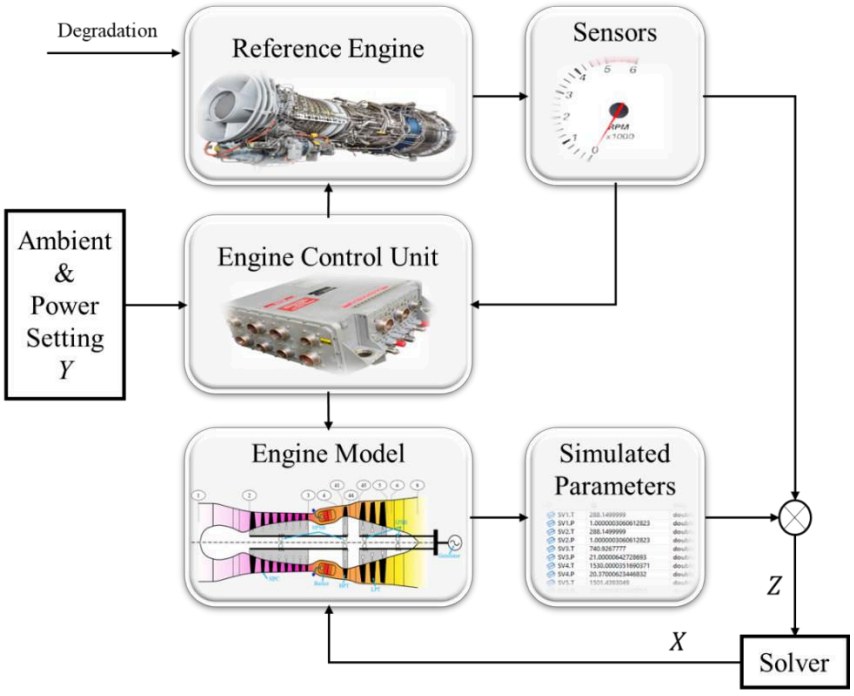


Fig. 5 Schematic of fault diagnosis [26].

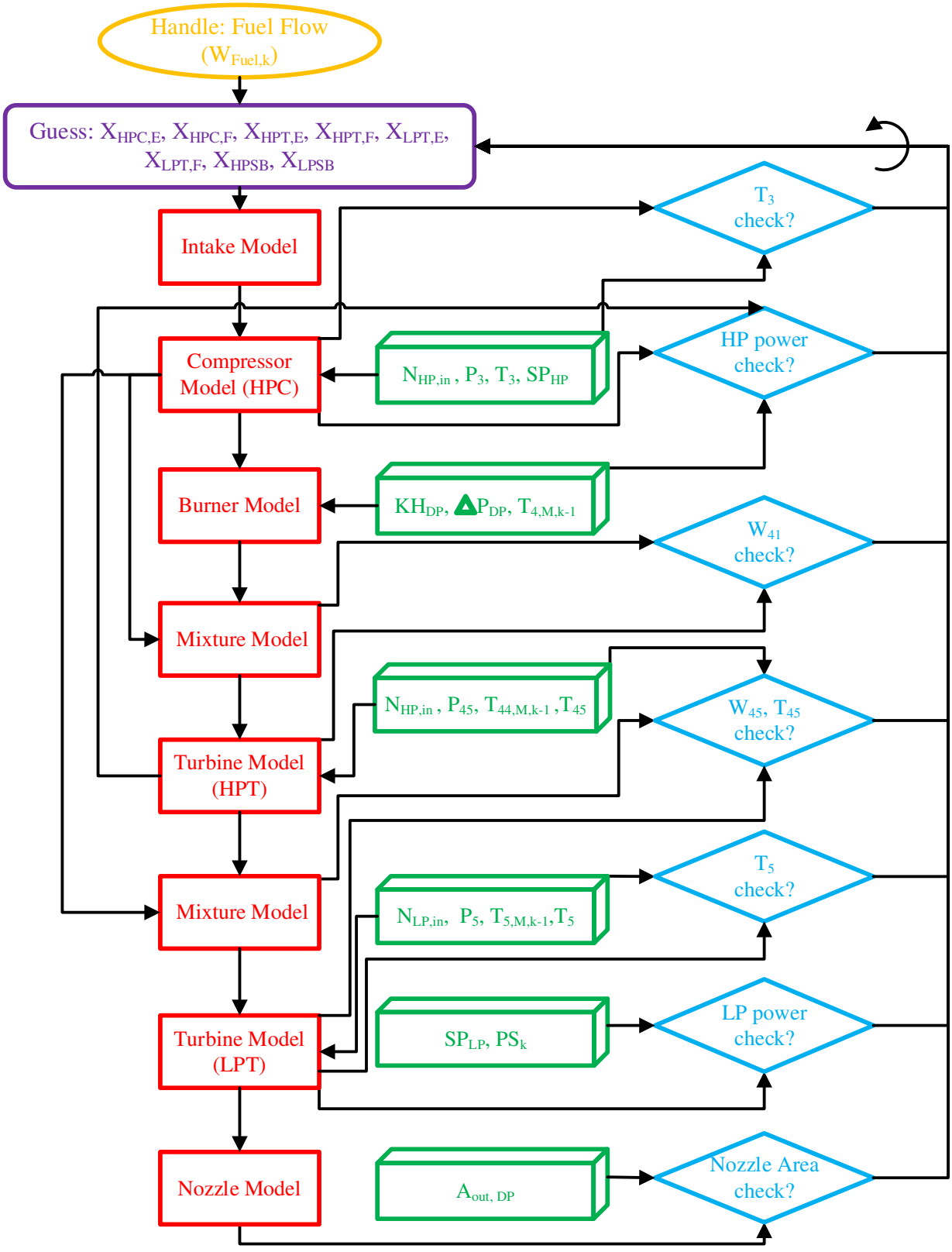


Fig. 6 Flowchart for fault diagnosis.

3. Engine Model Validation

The cutaway section of the relevant industrial gas turbine is shown in Fig. 2, similar to the GE LM2500+. The widely known commercial software GasTurb [51] was selected to validate the proposed engine model using hydrogen fuel for both transient and steady-state operation and to set the benchmark as a reference engine in the following sections. Table 3 shows the design point specification of the given dual-shaft engine.

Table 3 Design point specification of dual-shaft engine.

Operating Condition	Unit	Value
Engine Inlet Pressure	atm	1
Engine Inlet Temperature	Kelvin	288.15
Ambient Relative Humidity	%	60
Mass Flow Rate (Inlet Air)	kg/s	80
Fuel Flow Rate	kg/s	0.6560
Free Power Turbine Output	MW	31.98

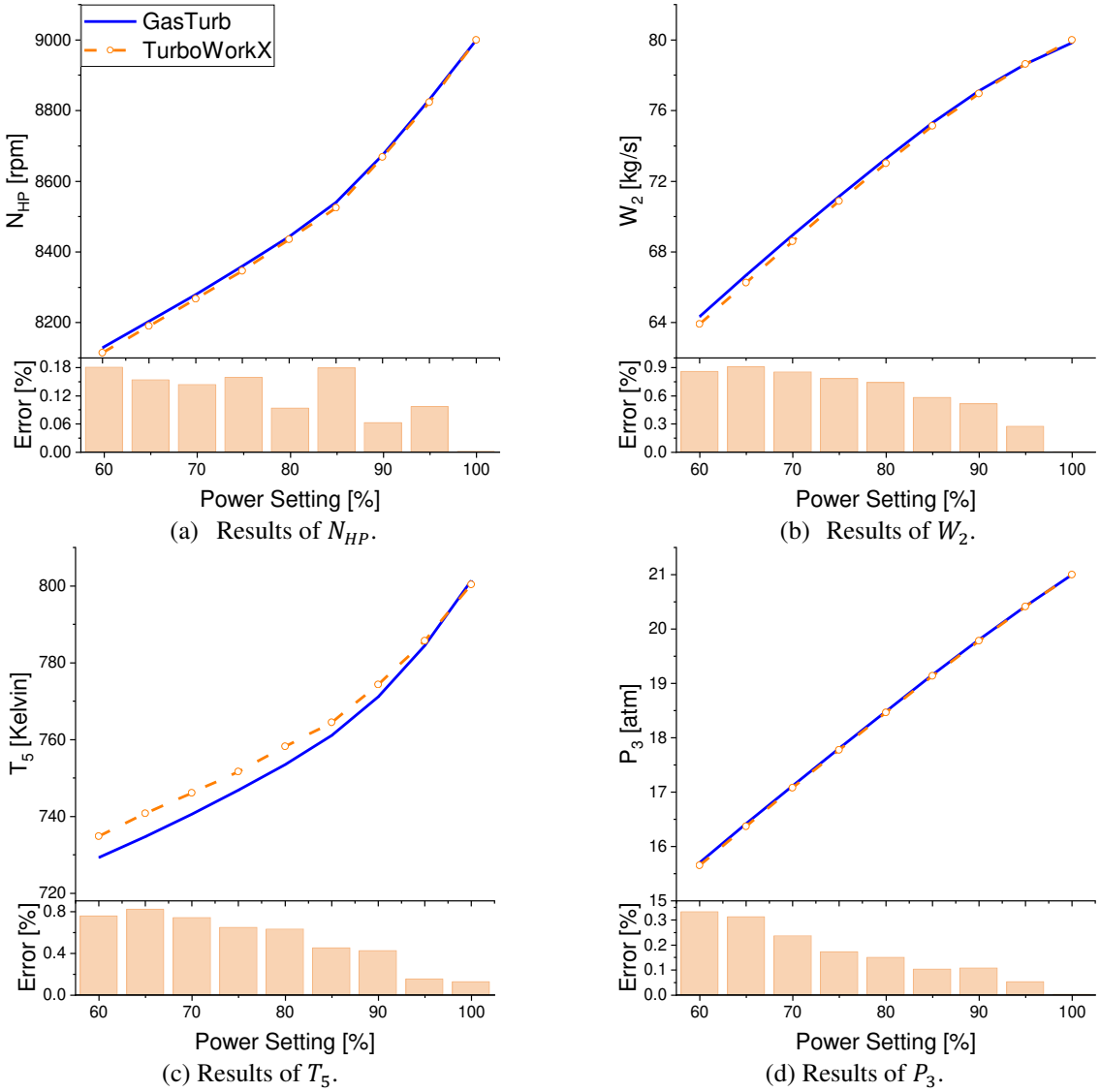
3.1 Model Validation at Steady-State Conditions

The engine must meet the demand fluctuations of the national grid not only at the design point of the engine but also at off-design points. Therefore, it is essential to validate the performance model of the engine at both design and off-design point conditions. Table 5 compares the results of GasTurb [51] and the developed model at design point conditions with the station number presented in Fig. 2, where the relative peak error is less than 0.395% for the different engine sections. It is apparent that the developed dual-shaft industrial gas turbine powered by hydrogen is comparable to the GasTurb at the design point.

Table 4 Comparison between GasTurb and developed model at design point [51].

Symbol	Units	GasTurb [51]	Developed Model	Relative Difference [%]
P_3	atm	21.00	21.00	0.000
T_3	Kelvin	739.87	740.93	0.143
P_4	atm	20.37	20.37	0.000
T_4	Kelvin	1500.00	1494.07	0.395
P_{45}	atm	5.09	5.09	0.000
T_{45}	Kelvin	1125.53	1127.78	0.200
P_5	atm	1.07	1.07	0.000
T_5	Kelvin	801.37	802.91	0.192
P_8	atm	1.05	1.05	0.000
T_8	Kelvin	801.37	802.91	0.192

The next stage of the validation is to examine off-design conditions, where the developed model and GasTurb [51] use the same com ponent maps, and both models use the "Engine Power" setting as the leading command condition. Here, for validation, the setting progresses from 60% to 100% in steps of 5%. Fig. 7 shows the results of comparing four of the simulation parameters for GasTurb and the TurboWorkX. More specifically, a variation in engine power setting is used to demonstrate *HP* rotational speed, inlet flow rate, turbine exit temperature, and outlet pressure of the compressor. Although the relative error increases with a decrease in power setting, the maximum error is less than 1%. The results support the notion that the developed gas turbine model is sufficient for simulation for both on- and off-design conditions. Hence, this proposed GPA algorithm will be implemented with the developed model to identify the main rotating components and the shaft bearing fault.



(a) Results of N_{HP}.

(b) Results of W_2.

(c) Results of T_5.

(d) Results of P_3.

Fig. 7 Model validation at off-design points.

3.2 Model Validation at Transient Conditions

A fundamental property of the GPA in unstable states is the ability to simulate engine performance under transient conditions. Hence, it is essential to validate the model developed here under transient conditions to help extend the foundation for GPA. For example, while performing a 15 seconds acceleration manoeuvre, the power setting goes up from 85% to 100%. After that, a deceleration of 15 seconds will be initiated, where the power setting is reduced from 100% back to 85%. Fig. 8 presents the fuel schedule obtained from GasTurb for these power settings over a 30-second interval. The developed model will simulate the transient behaviour for comparison and validation with GasTurb.

Four engine performance indicators were used in the established engine model and GasTurb with the relative error shown at the bottom of Fig. 9. It can be seen that the simulated parameters from the established engine model are consistent with GasTurb, with a relative peak error of less than 0.6%. The results suggest that the developed gas turbine engine model is sufficient for diagnosis under steady and transient conditions.

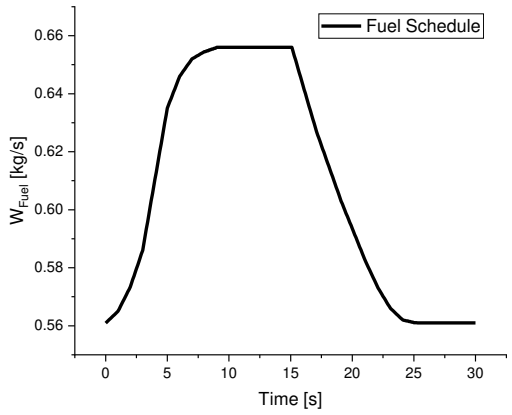
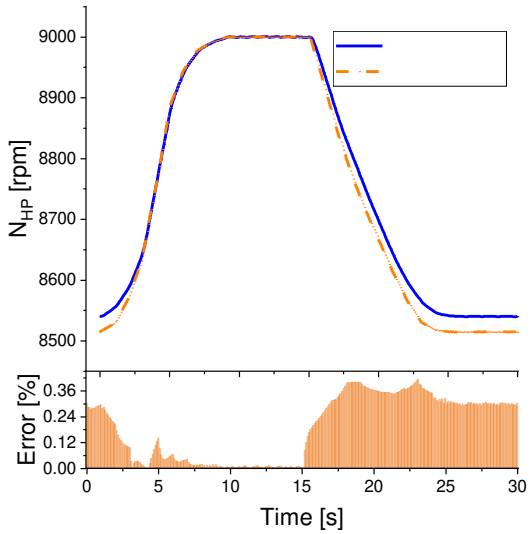
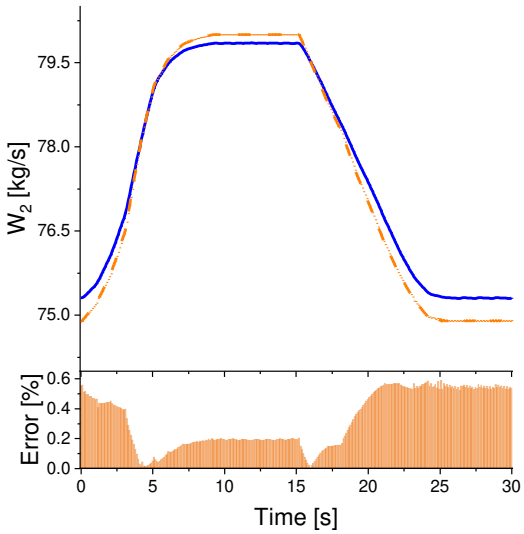


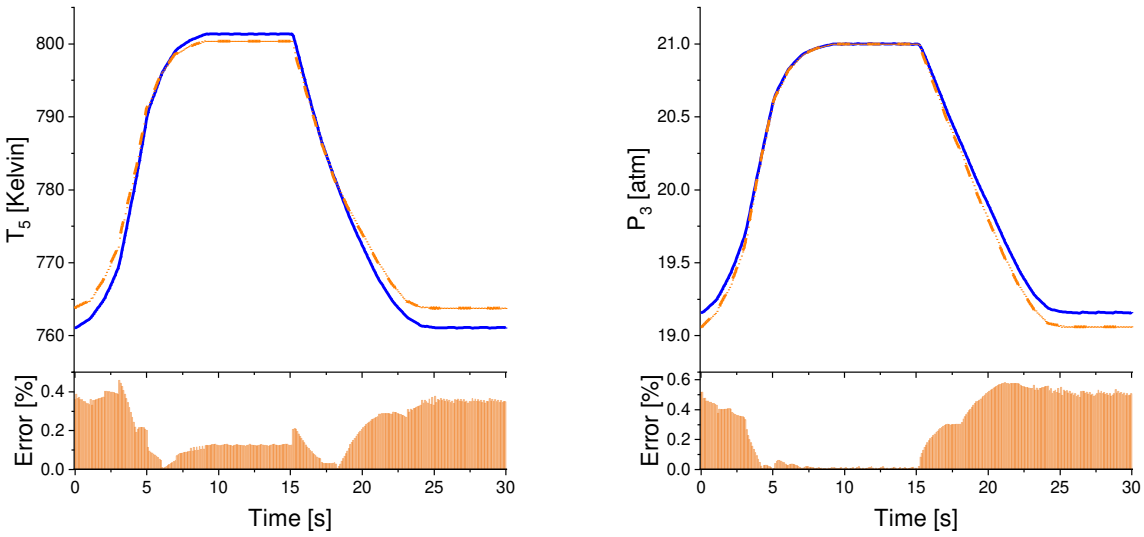
Fig. 8 Fuel schedule for model validation.



(a) Results of N_{HP}.



(b) Results of W_2.



(c) Results of T_5. (d) Results of P_3.

Fig. 9 Validation of model for transient manoeuvre.

4. Application and Analysis

Five case studies are presented to address each of the research questions in turn. The computation time is closely related to the computer specifications. Computing in these studies, for evaluation, was carried out on a personal computer with a typical i9 CPU @2.50GHz.

Case 1. The shaft bearing fault will be reflected not only in the vibration signal but also in an adverse effect on engine performance. This case study seeks to clarify the effect of faults in the HP and LP shaft bearings on performance parameters.

Case 2. This case study sets out to investigate how a shaft bearing failure may affect gas path analysis when the defect is not taken into account during steady-state fault identification.

Case 3. This case study seeks to examine the proposed gas path analysis method for compressor, turbine and shaft bearing faults at steady-state conditions.

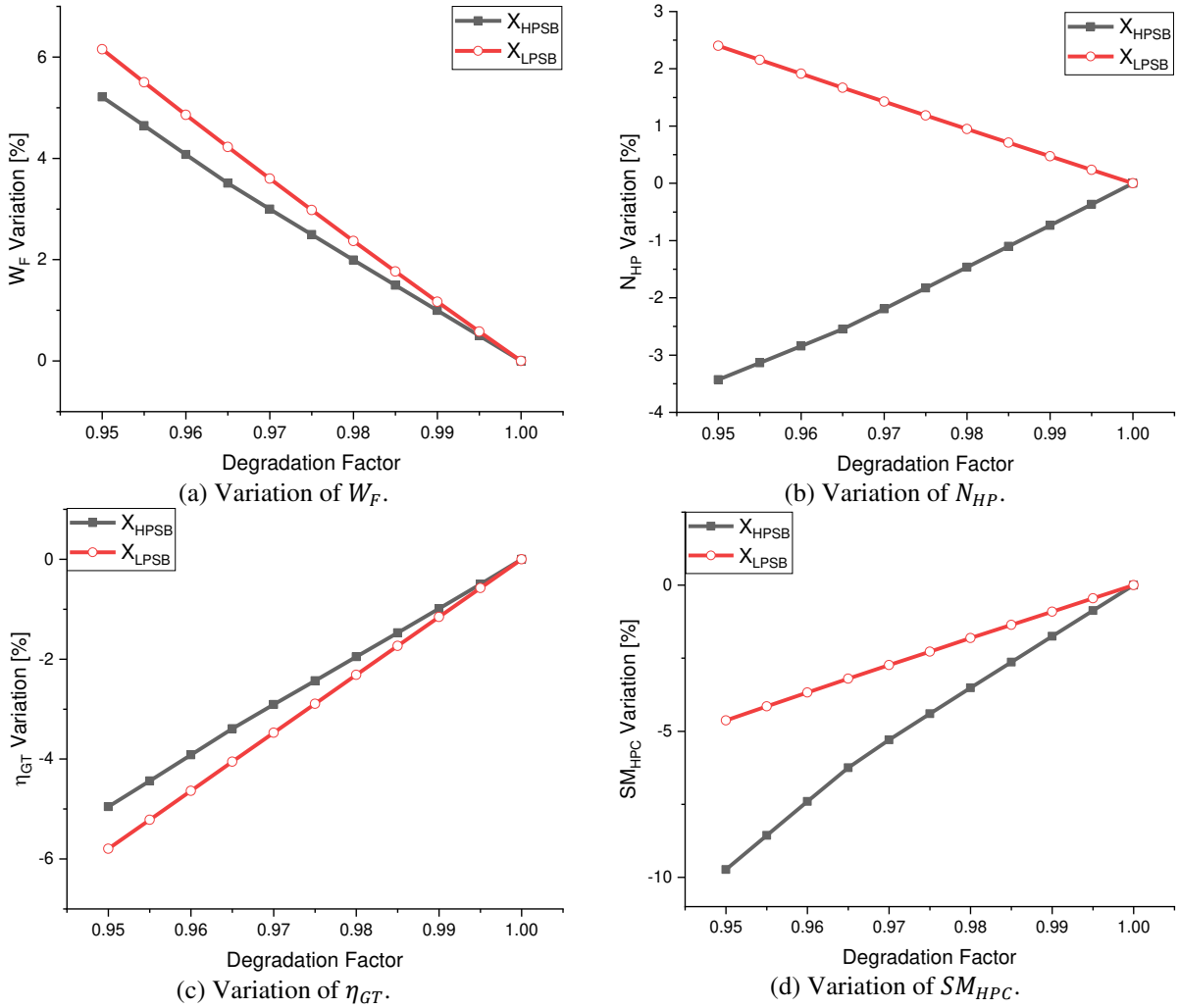
Case 4. It explores the effectiveness as well as the correctness of the proposed GPA method with a constant fault during a transient state and compares it with a state-of-the-art algorithm [20] to demonstrate convincing evidence of the benefits of the proposed method over the benchmark method.

Case 5. Aims to explore the robustness of the proposed GPA method when faced with a sudden failure during a transient manoeuvre.

4.1 Case 1: Effects of Shaft Bearing Fault on Engine Performance

An engine shaft bearing fault is a common phenomenon during the life cycle of a gas turbine. A shaft bearing fault will cause a deterioration in the mechanical efficiency of the spool for the HP and LP spools, respectively. The degradation due to the HP and LP shaft bearing faults are presented in Fig. 10. Here, the ambient conditions and power setting are assumed to be the same as the baseline condition. To explore the effect of the shaft bearing fault on engine performance, the design point was chosen to be the reference state. The state of health of the shaft bearing is represented by X_{HPSB}, and X_{LPSB}, both of which are equal to 1 in Fig. 10.

It can be seen in Fig. 10 (a) that the presence of the shaft bearing fault will increase fuel consumption (W_F) to maintain the design point power output. The $LPSB$ fault will increase the compressor rotation speed (N_{HP}) as W_F is increased in Fig. 10 (b). In contrast, the $HPSB$ fault will decrease N_{HP}, as more of the power generated by the HPT is consumed by the $HPSB$. Although the increasing of W_F could increase the N_{HP} to some extent, the power imbalance between HPC and HPT casued by $HPSB$ is dominant. It is worth noting that the corrected rotational speed of the HPC (CN_{HPC}) in compressor map has the same tendency with N_{HP} as the inlet condition is the same as the healthy state. Fig. 10 (c) indicates that the decrease in engine thermal efficiency (η_{GT}) caused by the $LPSB$ fault has a greater effect than the $HPSB$ fault. This is because the compressor efficiency improves when CN_{HPC} decreases below 1, and becomes worse when CN_{HPC} increases above 1 in the selected compressor map [52]. In addition, it is seen in Fig. 10 (a) that the W_F required with the $LPSB$ fault is higher than with the $HPSB$ fault. Fig. 10 (d) shows that that the effect of the $HPSB$ fault on SM_{HPC} is substantial, and that the presence of either or both the $HPSB$ and $LPSB$ faults will reduce the compressor surge margin (SM_{HPC}). More precisely, the HP shaft bearing degradation could be treated as HP shaft power extraction, which requires more fuel to maintain the same engine power output. The increase in fuel consumption will result in the increase of T_4/T_2, which will cause the compressor working line moving closer to the surge margin. In contrast, the LP shaft bearing fault could be regarded as extra engine power output needed, which acted as increasing the power setting of the gas turbine. Hence, the compressor working point will shift to the upper right under the steady-state compressor working line. Accordingly, the surge margin will be lowered, because the compressor operating point will approach the surge line when the speed line exceeds one and when suffering from LP shaft bearing degradation.



(a) Variation of W_F.

(b) Variation of N_{HP}.

(c) Variation of η_{GT}.

(d) Variation of SM_{HPC}.

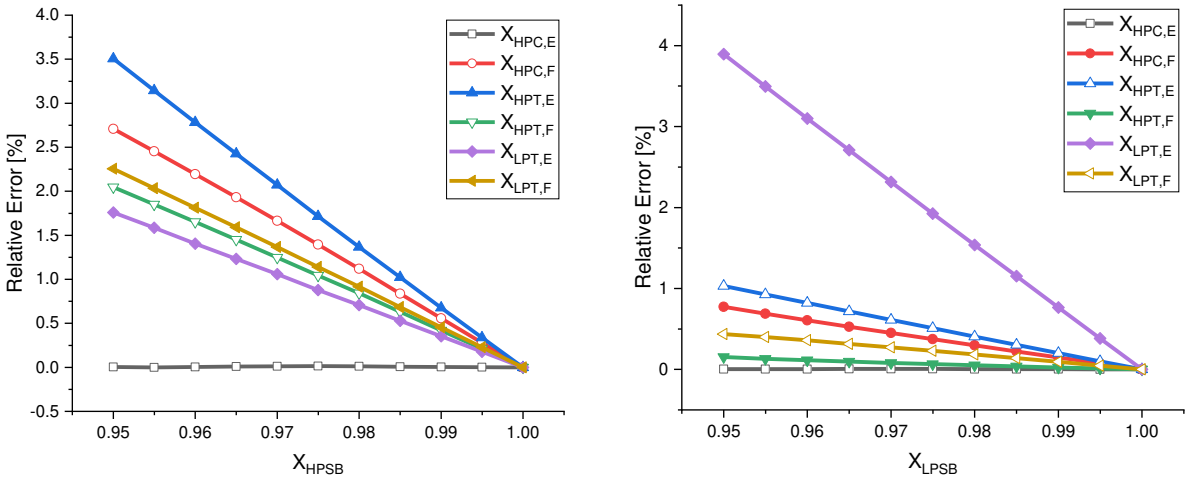
Fig. 10 Effect of shaft bearing fault on engine performance.

4.2 Case 2: Effects of Shaft Bearing Fault on Gas Path Analysis at Steady-State Conditions

The preceding case study has elucidated the impact of shaft bearings on engine gas path parameters and performance. However, the effect of gas path parameter deviation due to shaft bearing faults on gas path analysis remains unanswered. This case study injected the HP and LP shaft bearing degradation separately and kept the three rotational components healthy to generate the faulty gas path measurements. Then, the measures are applied to gas path analysis to identify the health condition of three rotational components and quantify the levels of those previous studies that ignored the shaft bearing fault in fault diagnosis.

Fig. 11 (a) shows the effect of HP shaft bearing deterioration (X_{HPSB}) on gas path analysis when the shaft bearing problem is ignored. As can be seen, the $X_{HPT,E}$ is most susceptible where the maximum relative error is around 3.5%. If the shaft bearing issue is disregarded, Fig. 11 (b) illustrates how LP shaft bearing degeneration affects gas path

analysis. It is evident that the most significant relative error of approximately 3.89% is where the $X_{LPT,E}$ is most vulnerable. It is clearly to see that the maximum relative error caused by LP shaft bearing degradation is larger than HP shaft bearing degradation. This is because the LP shaft bearing degradation is more sensitive than the HP shaft bearing fault, as depicted in the previous case study (Fig. 10 (c)). The results show that the fault diagnosis will be biased and may raise a false alert if shaft bearing degradation is ignored during fault identification.



(a) Fault diagnosis error caused by X_{HPSB} (b) Fault diagnosis error caused by X_{LPSB}

Fig. 11 Effect of shaft bearing fault on gas path analysis.

4.3 Case 3: Gas Path Analysis at Steady-State Conditions

The basic requirement of GPA is the ability to diagnose the health status of the engine effectively under steady-state operating conditions. Thus, it is worth verifying the prediction accuracy and diagnostic time of the proposed scheme under steady-state conditions first during fault development and propagation. The flow chart proposed for the GPA can be seen in Fig. 6, where dynamic effect compensation is still active, although there is little or no dynamic effect. The fault propagation model described in Eq. **(2)** is applied to introduce faults into the healthy condition, 'Health State I' shown in Table 2, to represent the likely fault amplitude after 25,000 $EFLH$.

Fig. 12 compares the actual fault with the predicted fault and its propagation. The proposed GPA was found to track the actual fault with high precision even if the fault changes with $EFLH$. The average run time, average diagnosis error, and maximum error when using GPA with fault propagation during the engine life cycle are 0.1064 s, 0.0014%, and 0.0086%, respectively. The methodology shows high precision in real-time when detecting the given engine faults over the entire life cycle.

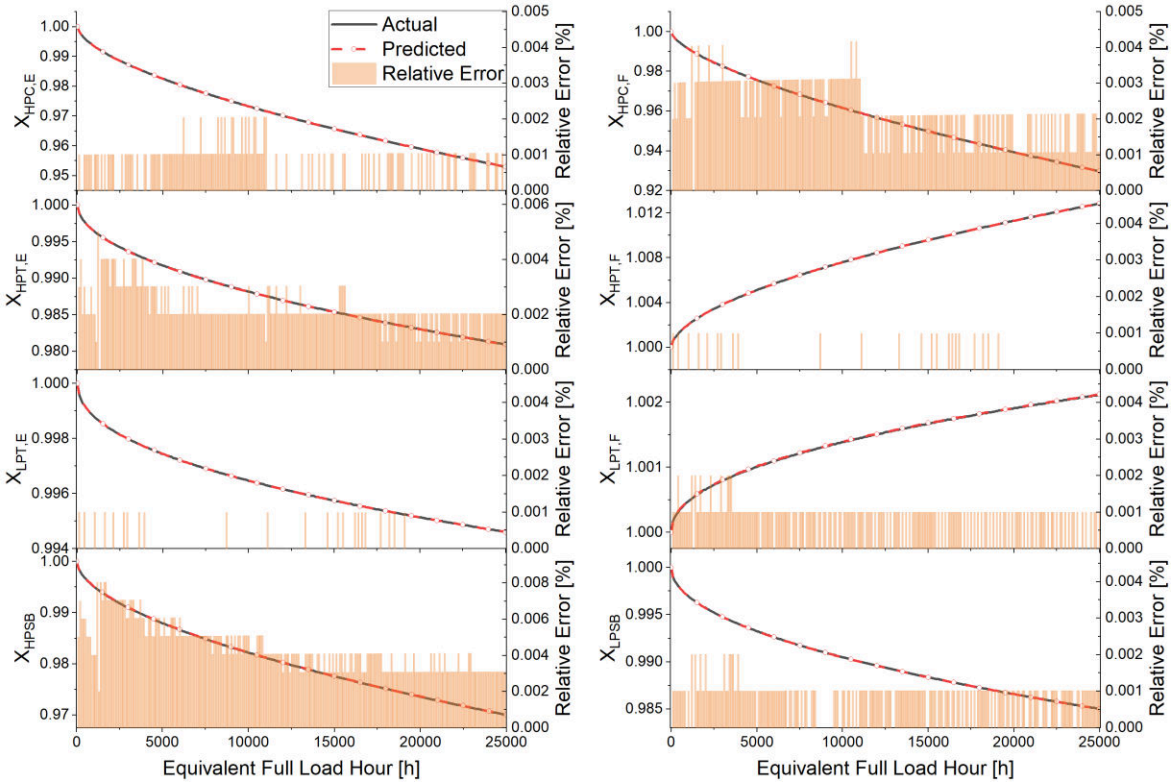
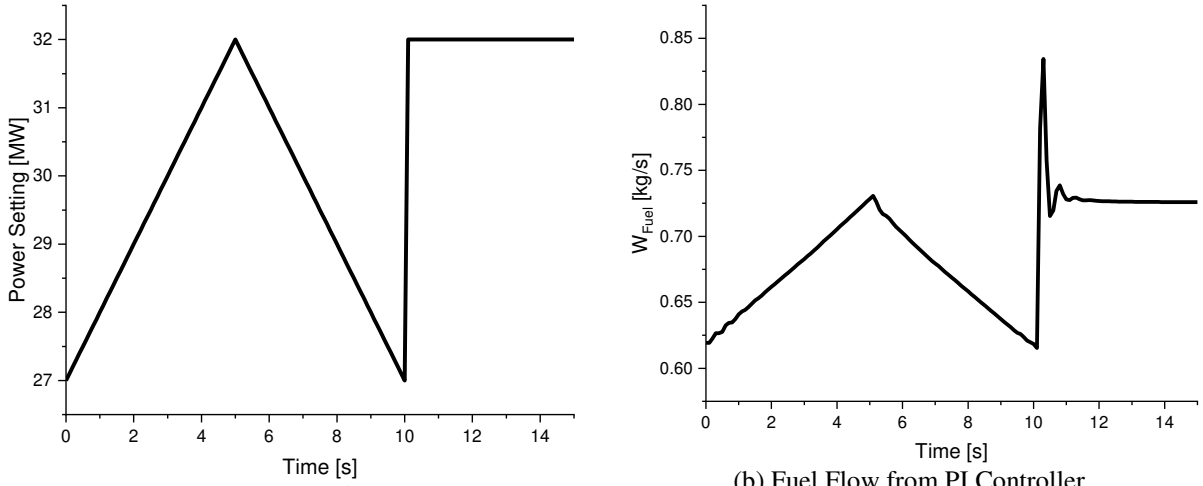


Fig. 12 Actual and predicted degradation factors with fault propagation with *EFLH*.

4.4 Case 4: Gas Path Analysis with Constant Health State during Transient Manoeuvre

Nowadays, industrial gas turbines are expected to operate for prolonged periods of time under dynamic conditions, so there is a need to evaluate their health during their operation. Case 3 examines the capacity of the developed process for continuous GPA under transient events. Fig. 13 (a) represents the power setting for 15 s duration, with the simulation time step 0.1 s. Fig. 13 (b) shows the corresponding engine fuel flow from the PI controller.



(a) Power Setting.

(b) Fuel Flow from PI Controller.

Fig. 13 Power Setting and fuel flow during transient 15 s manoeuvre.

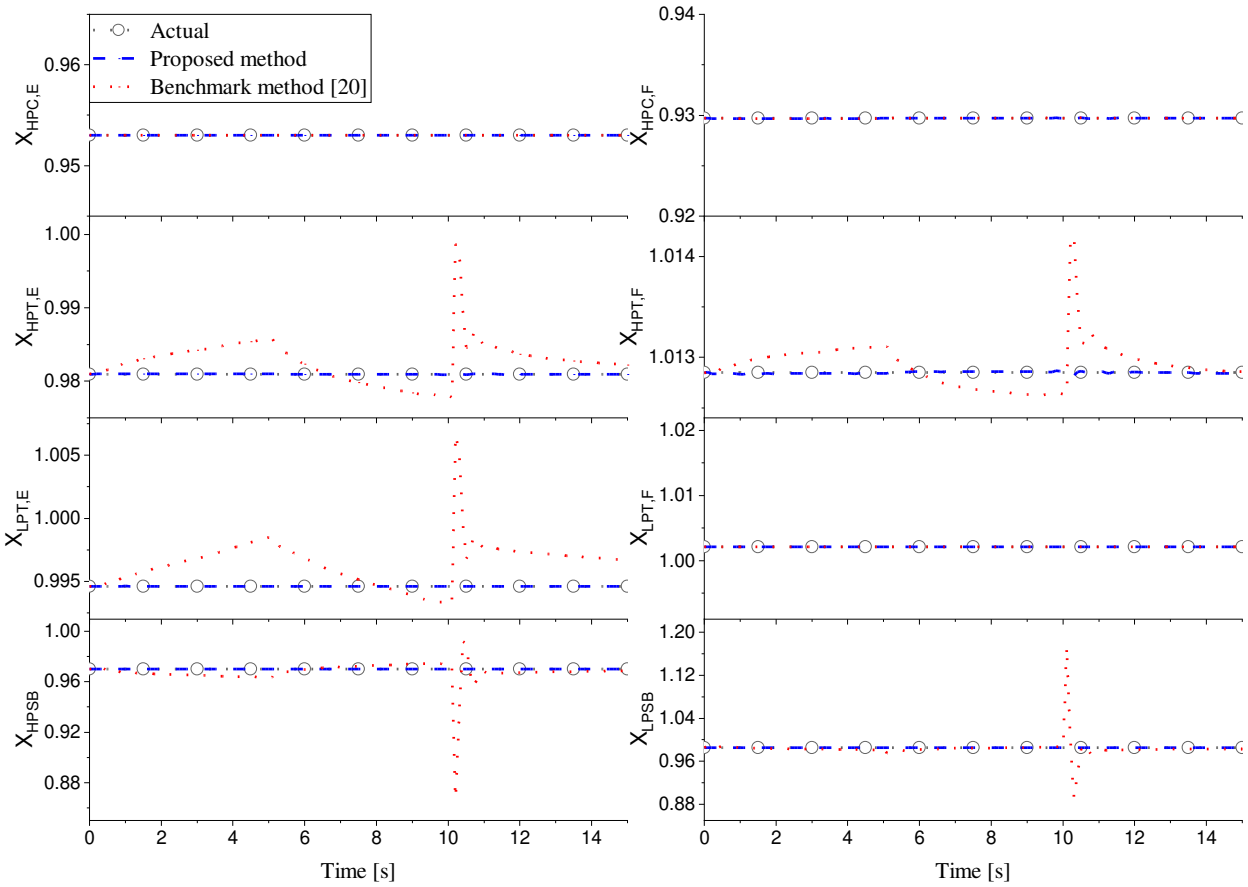


Fig. 14 Results of fault diagnosis with constant rate of degradation during a 15 s transient manoeuvre.

The results during the 15 s manoeuvre using the proposed GPA method and benchmark method [20] are shown in Fig. 14 and the relative diagnostic error is in Fig. 15. It is evident that the proposed method performs better than the benchmark method, with peak errors of 0.013% and 19.123% for the proposed approach and the benchmark technique, respectively. It is seen in Fig. 13 (b) that the faster the engine fuel flow changes, the larger the diagnosis error for the benchmark approaches. When the engine is operating transiently using the benchmark approach, the condition monitoring system may likely provide fluctuation data and generate false alerts. In contrast, the slam operation does affect the diagnostic accuracy of the proposed method, but the peak error is only 0.013%, as mentioned above. For the proposed method, the average computation time and average relative error for each time instant during the transient manoeuvre are 0.1152 s and 0.0014%, respectively. Here, the computational time is the time for execution of the fault diagnosis at each time step. It follows that excellent results and accuracy were achieved in fault identification with the proposed real-time monitoring technique.

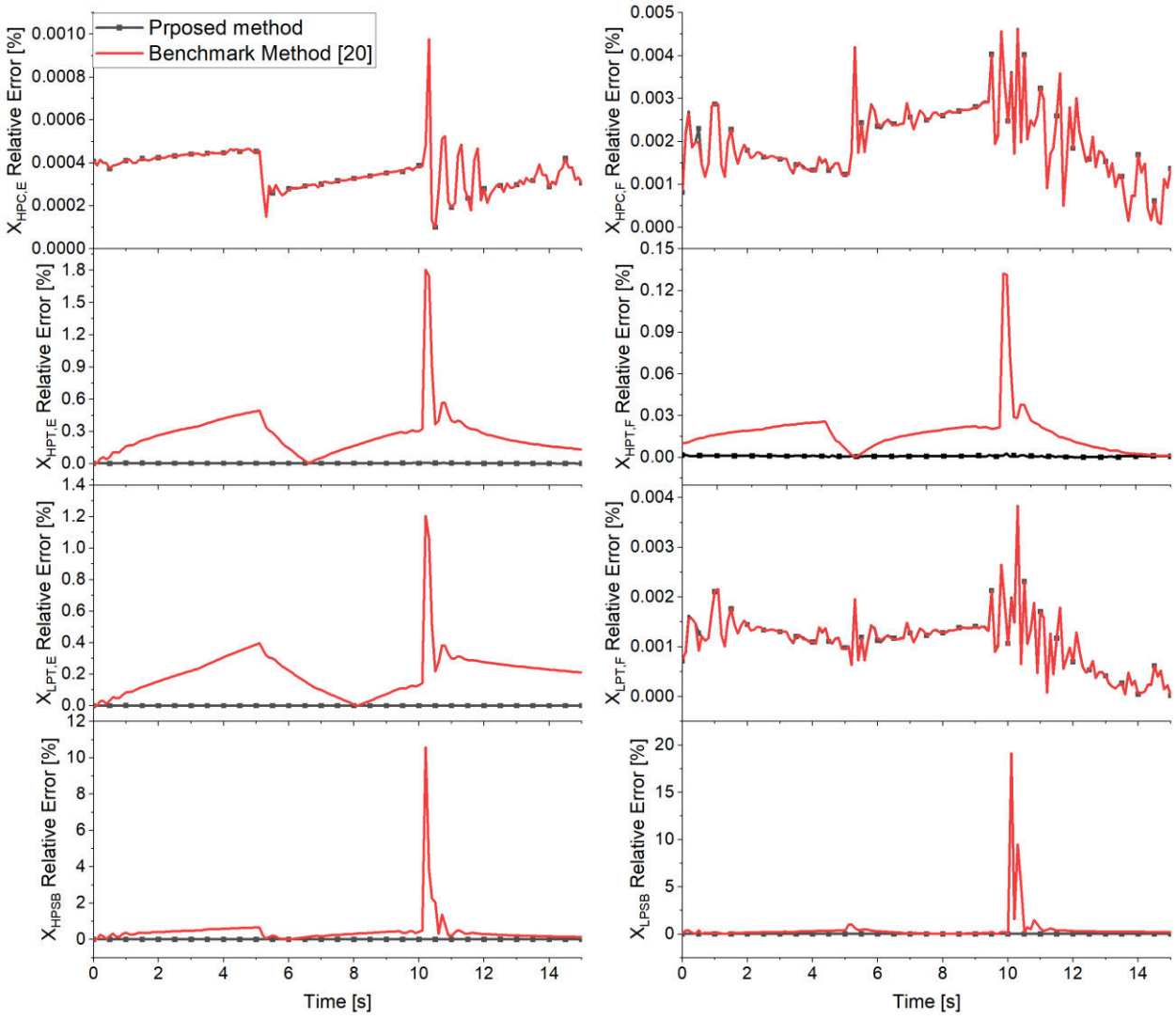
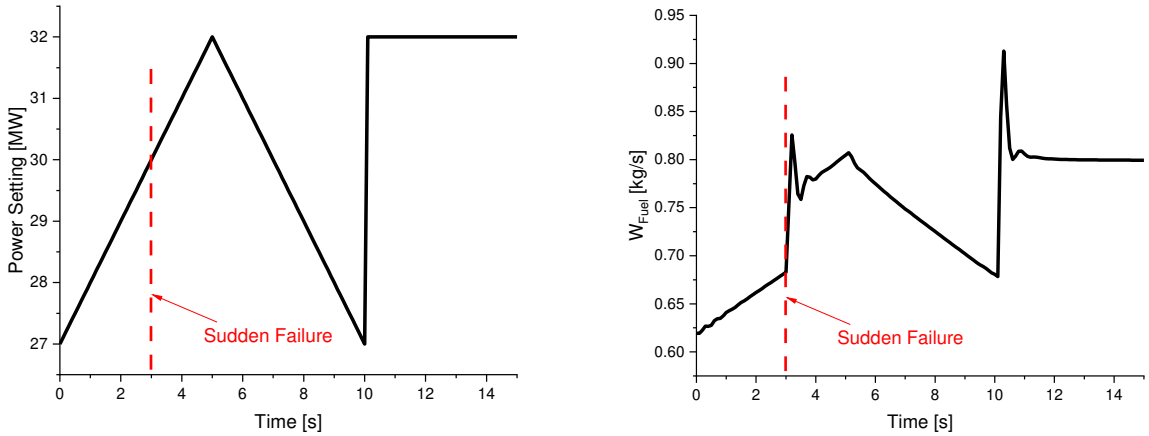


Fig. 15 Relative error of fault diagnosis with constant rate of degradation during a 15 s transient manoeuvre.

4.5 Case 5: Gas Path Analysis with Sudden Failure during Transient Manoeuvre

The likelihood of sudden failure of a gas turbine cannot be entirely avoided under dynamic conditions. If the GPA cannot cope with sudden faults occurring during a dynamic manoeuvre, there would be no benefit in conducting fault diagnosis under dynamic conditions. Hence, it is essential to verify that the methodology can cope with a surge failure that occurs during a dynamic manoeuvre. Fig. 16 (a) illustrates the power setting during a 15 s duration, the same as Case 3. In contrast, the engine fuel flow shown in Fig. 16 (b) is different from previously as it must compensate for the sudden failure that occurs at a time of 3 s. Because the previous case study shows that the suggested technique is superior to the benchmark method, this case study will only provide the findings obtained using the proposed method.



(a) Power Setting. (b) Fuel Flow from PI Controller.

Fig. 16 Power setting and fuel flow during a transient manoeuvre with sudden failure.

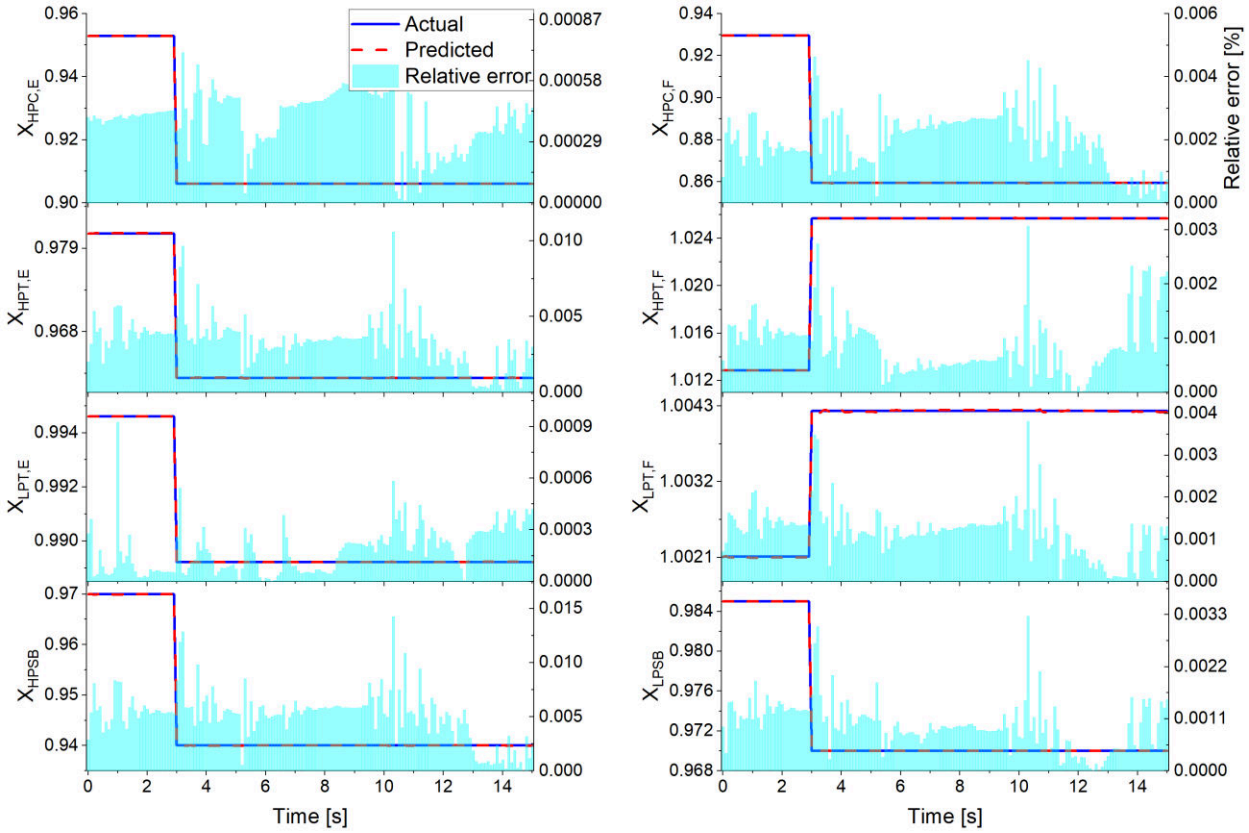


Fig. 17 Relative error of fault diagnosis with sudden failure during a 15 s transient manoeuvre.

Fig. 17 presents the comparative error of all eight degeneration factors over a 15 s operating period. The peak error is found at 10.3 s which is 0.0143% for X_{HPSB}, which is the same time instant as for Case 3. The reason is the mechanics of the slam operation and its subsequent dynamic effect. Although the maximum error increases slightly from 0.0128% to 0.0143% compared to Case 3, the GPA results are within reasonable accuracy. The average computed

time for each instant and the average diagnostic error during a transient manoeuvre with sudden failure is 0.1158 s and 0.0014%, respectively.

The results demonstrate and illustrate that degradations in the shaft bearing may have a discernible impact on the performance of gas turbines and, as a result, affect gas path measurements. In addition, the results reveal that the shaft bearing degradation will have a negative effect on fault identification, if the gas path analysis only focuses on the major rotational components of the gas turbine.

It is a well-known fact that the quantification of engine faults cannot be measured directly. Hence, the quantification results should be derived from gas path measurement in an inverse mathematical manner. In this research, the iteration is engaged to tune the degradation factors until the predicted parameters are aligned with the measured parameters. Based on the proposed method, sudden failures of main rotating components and shaft bearings could be identified in real-time, which will greatly improve the health monitoring capabilities of gas turbine engines and avoid catastrophic consequences.

5. Conclusions

The study was undertaken to explore the effect of shaft bearing faults on performance and gas path analysis and evaluate the proposed method for identifying both engine component and shaft bearing faults simultaneously through the evaluation of dynamic effects on the operation of the system. The findings from this study were verified with the proposed GPA. The results demonstrated that both main components and shaft bearing faults were accurately predicted in real-time, including the occurrence of sudden transient failures.

The conclusions drawn from this study are as follows:

- The developed engine model has been validated with the engineering software GasTurb for both transient and steady-state conditions where peak error is less than 1% for all test cases.
- The LP shaft bearing fault has a more severe impact on engine thermal efficiency than the HP shaft bearing fault for the same power output. In contrast, the negative effect of LP shaft bearing fault on the surge margin is less than that of HP.
- This work has shown that shaft bearing deterioration should not be ignored in gas path analysis; when HP and LP shaft bearing faults are omitted, the largest fault diagnostic error is 3.5% and 3.89%, respectively.

- The maximum mean relative error between the predicted fault and implanted fault of the proposed GPA for main rotating components and shaft bearing fault diagnosis under steady-state conditions was less than 0.0086%. The average computation time for each diagnosis was 0.1064 s, which could be used for real-time condition monitoring.
- For the GPA under transient conditions, the peak mean relative errors for a constant rate of degradation and sudden failure were 0.0128% and 0.0143%, respectively, with respective average computing times of only 0.1152 s and 0.1158 s.

Prior to this study, it had not been possible to identify sudden shaft bearing faults occurring under dynamic conditions by GPA. Furthermore, this study thoroughly investigates how shaft bearings affect engine performance and GPA. The present study does make several distinct contributions to the GPA of gas turbines under both transient and steady-state conditions. A key benefit of this study was to demonstrate that the proposed GPA method could simultaneously identify faults in the main rotating components and shaft bearings of the engine.

Overall, this study gives a new insight into the application of GPA to industrial gas turbines, with the potential to improve engine reliability through condition-based maintenance. The quantification evaluation of shaft bearing failure on engine performance metrics and GPA results is another significant advantage of the current study. The available statistics emphasise the importance of including the shaft bearing fault in gas path calculations.

Acknowledgements

The authors acknowledge the support of the Propulsion and Space Research Center (PSRC) of the Technology Innovation Institute (TII) in Abu Dhabi, United Arab Emirates.

Appendix A

Table A- 1 Fault propagation coefficients for Health Status I.

Component	Symbol		Degradation Factor	m	n
HPC	X_{HPC}	$X_{HPC,E}$	*HPC* efficiency index	0.00010	0.6053
		$X_{HPC,F}$	*HPC* flow capacity index	0.00010	0.6440
HPT	X_{HPT}	$X_{HPT,E}$	*HPT* efficiency index	0.00010	0.5175
		$X_{HPT,F}$	*HPT* flow capacity index	0.00004	0.5694
LPT	X_{LPT}	$X_{LPT,E}$	*LPT* efficiency index	0.00005	0.4619
		$X_{LPT,F}$	*LPT* flow capacity index	0.00002	0.4601
$HPSB$	X_{HPSB}		HP shaft mechanical efficiency index	0.00010	0.5618

$LPSB$	X_{LPSB}	LP shaft mechanical efficiency index	0.00010	0.4941

References

[1] Tahan M, Tsoutsanis E, Muhammad M, Abdul Karim ZA. Performance-based health monitoring, diagnostics and prognostics for condition-based maintenance of gas turbines: A review. Applied Energy 2017;198:122–44.

[2] Kordestani M, Orchard ME, Khorasani K, Saif M. An Overview of the State of the Art in Aircraft Prognostic and Health Management Strategies. IEEE Trans Instrum Meas 2023;72:1–15.

[3] Tsoutsanis E. A dynamic prognosis scheme for flexible operation of gas turbines. Applied Energy 2016.

[4] Urban LouisA. Gas Turbine Engine Parameter Interrelationships. Hamilton Standard Division of United Aircraft Corporation; 1969.

[5] Shirizadeh B, Quirion P. The importance of renewable gas in achieving carbon-neutrality: Insights from an energy system optimization model. Energy 2022;255:124503.

[6] Zhou Y, Ma Z, Shi X, Zou S. Multi-agent optimal scheduling for integrated energy system considering the global carbon emission constraint. Energy 2024;288:129732.

[7] Xiong Y, Zeng Z, Xin J, Song G, Xia Y, Xu Z. Renewable energy time series regulation strategy considering grid flexible load and N-1 faults. Energy 2023;284:129140.

[8] Tsoutsanis E, Hamadache M, Dixon R. Real-Time Diagnostic Method of Gas Turbines Operating Under Transient Conditions in Hybrid Power Plants. Journal of Engineering for Gas Turbines and Power 2020;142:101002.

[9] Tsoutsanis E, Meskin N. Derivative-driven window-based regression method for gas turbine performance prognostics. Energy 2017;128:302–11.

[10] Li J, Ying Y. A Method to Improve the Robustness of Gas Turbine Gas-Path Fault Diagnosis Against Sensor Faults. IEEE Transactions on Reliability 2018;67:3–12.

[11] Hanachi H, Liu J, Kim IY, Mechefske CK. Hybrid sequential fault estimation for multi-mode diagnosis of gas turbine engines. Mechanical Systems and Signal Processing 2019;115:255–68.

[12] Montazeri-Gh M, Yazdani S. Application of interval type-2 fuzzy logic systems to gas turbine fault diagnosis. Applied Soft Computing 2020;96:106703.

[13] Chen Y, Zhao X, Xiang H, Tsoutsanis E. A sequential model-based approach for gas turbine performance diagnostics. Energy 2021;220:119657.

[14] Mantelli L, Zaccaria V, Ferrari ML, Kyprianidis K. A Degradation Diagnosis Method for Gas Turbine—Fuel Cell Hybrid Systems Using Bayesian Networks. Journal of Engineering for Gas Turbines and Power 2021;143:054502.

[15] Zhao J, Li Y-G, Sampath S. A hierarchical structure built on physical and data-based information for intelligent aero-engine gas path diagnostics. Applied Energy 2023;332:120520.

[16] Sampath S, Ogaji SOT, Li YG, Singh R. Fault diagnosis of a two spool turbo-fan engine using transient data: A genetic algorithm approach. American Society of Mechanical Engineers, International Gas Turbine Institute, Turbo Expo, vol. 1, 2003, p. 351–9.

[17] Li YG. A gas turbine diagnostic approach with transient measurements. Proceedings of the Institution of Mechanical Engineers, Part A: Journal of Power and Energy 2003;217:169–78.

[18] Mousavi M, Chaibakhsh A, Jamali A, Kordestani M, Saif M. A New Fault Diagnosis Approach for Heavy-Duty Gas Turbines. IEEE/ASME Trans Mechatron 2022;27:3339–49.

[19] Amirkhani S, Tootchi A, Chaibakhsh A. Fault detection and isolation of gas turbine using series–parallel NARX model. ISA Transactions 2022;120:205–21.

[20] Ying Y. An improved performance diagnostic method for industrial gas turbines with consideration of intake and exhaust system. Applied Thermal Engineering 2023.

[21] Wang F, Deng G, Liu C, Su W, Han Q, Li H. A deep feature extraction method for bearing fault diagnosis based on empirical mode decomposition and kernel function. Advances in Mechanical Engineering 2018;10:168781401879825.

[22] Zhao H, Liao Z, Liu J, Li M, Liu W, Wang L, et al. A highly robust thrust estimation method with dissimilar redundancy framework for gas turbine engine. Energy 2022;245:123255.

[23] Park Y, Choi M, Choi G. Fault detection of industrial large-scale gas turbine for fuel distribution characteristics in start-up procedure using artificial neural network method. Energy 2022;251:123877.

[24] Li YG. Gas turbine performance and health status estimation using adaptive gas path analysis. Journal of Engineering for Gas Turbines and Power 2010;132:1–9.
[25] Saxena A, Goebel K, Simon D, Eklund N. Damage propagation modeling for aircraft engine run-to-failure simulation. 2008 International Conference on Prognostics and Health Management, PHM 2008 2008.
[26] General Electric. The LM2500+ Engine 2023. www.geaerospace.com/propulsion/marine/lm2500-plus (accessed June 12, 2023).
[27] Verbist M. Gas path analysis for enhanced aero-engine condition monitoring and maintenance. Delft University of Technology, 2017.
[28] Chen Y-Z, Tsoutsanis E, Xiang H-C, Li Y-G, Zhao J-J. A dynamic performance diagnostic method applied to hydrogen powered aero engines operating under transient conditions. Applied Energy 2022;317:119148.
[29] Kurzke J, Halliwell I. Propulsion and Power: An Exploration of Gas Turbine Performance Modeling. Cham, Switzerland: Springer International Publishing AG, part; 2018.
[30] Park Y, Choi M, Kim K, Li X, Jung C, Na S, et al. Prediction of operating characteristics for industrial gas turbine combustor using an optimized artificial neural network. Energy 2020;213:118769.
[31] Tsoutsanis E, Qureshi I, Hesham M. Performance diagnostics of gas turbines operating under transient conditions based on dynamic engine model and artificial neural networks. Engineering Applications of Artificial Intelligence 2023;126:106936.
[32] Chen Y-Z, Li Y-G, Tsoutsanis E, Newby M, Zhao X-D. Techno-economic evaluation and optimization of CCGT power Plant: A multi-criteria decision support system. Energy Conversion and Management 2021;237:114107.
[33] Wei Z, Zhang S, Jafari S, Nikolaidis T. Self-enhancing model-based control for active transient protection and thrust response improvement of gas turbine aero-engines. Energy 2022;242:123030.
[34] Pang S, Li Q, Feng H. A hybrid onboard adaptive model for aero-engine parameter prediction. Aerospace Science and Technology 2020;105:105951.
[35] Chatterjee S, Litt JS. Online model parameter estimation of jet engine degradation for autonomous propulsion control. AIAA Guidance, Navigation, and Control Conference and Exhibit, Austin, Texas, USA: 2003, p. 1–17.
[36] Ying Y, Li J. An improved performance diagnostic method for industrial gas turbines with consideration of intake and exhaust system. Applied Thermal Engineering 2023;222:119907.
[37] Tsoutsanis E, Meskin N. Dynamic performance simulation and control of gas turbines used for hybrid gas/wind energy applications. Applied Thermal Engineering 2019;147:122–42.
[38] Wei Z, Jafari S, Zhang S, Nikolaidis T. Hybrid Wiener model: An on-board approach using post-flight data for gas turbine aero-engines modelling. Applied Thermal Engineering 2021;184:116350.
[39] Zhou D, Yao Q, Wu H, Ma S, Zhang H. Fault diagnosis of gas turbine based on partly interpretable convolutional neural networks. Energy 2020;200:117467.
[40] Singh R, Maity A, Nataraj PSV. Dynamic modeling and robust nonlinear control of a laboratory gas turbine engine. Aerospace Science and Technology 2022:107586.
[41] Kim S. A new performance adaptation method for aero gas turbine engines based on large amounts of measured data. Energy 2021;221:119863.
[42] Sheng H, Chen Q, Li J, Jiang W, Wang Z, Liu Z, et al. Research on dynamic modeling and performance analysis of helicopter turboshaft engine's start-up process. Aerospace Science and Technology 2020;106:106097.
[43] Wang C, Li YG, Yang BY. Transient performance simulation of aircraft engine integrated with fuel and control systems. Applied Thermal Engineering 2017;114:1029–37.
[44] Wang T, Zhang Y, Yin Z, Qiu L, Hua Y, Zhang X, et al. Decoupling control scheme optimization and energy analysis for a triaxial gas turbine based on the variable power offtakes/inputs. Energy 2023;262:125560.
[45] Wang T, Zhang Y, Yin Z, Zhang H, Qian Y. Energy analysis and control scheme optimizations for a recuperated gas turbine with variable power offtakes/inputs. Energy 2023;285:129383.
[46] Walsh PP, Fletcher P. Gas turbine Performance. Oxford: Blackwell Science; 2004.
[47] Li Z, Li Y-G, Sampath S. Aeroengine transient performance simulation integrated with generic heat soakage and tip clearance model. Aeronaut j 2022:1–23.
[48] Chen Y-Z, Tsoutsanis E, Wang C, Gou L-F. A time-series turbofan engine successive fault diagnosis under both steady-state and dynamic conditions. Energy 2023;263:125848.
[49] Park Y, Choi M, Choi G. Fault detection of industrial large-scale gas turbine for fuel distribution characteristics in start-up procedure using artificial neural network method. Energy 2022;251:123877.
[50] Hu Y, Sun Z, Cao L, Zhang Y, Pan P. Optimization configuration of gas path sensors using a hybrid method based on tabu search artificial bee colony and improved genetic algorithm in turbofan engine. Aerospace Science and Technology 2021;112:106642.

[51] Kurzke J. GasTurb: A Program to Calculate Design and Off-Design Performance of Gas Turbines 2017.
[52] Tsoutsanis E. A component map tuning method for performance prediction and diagnostics of gas turbine compressors. Applied Energy 2014.



https://dspace.org/

An advanced performance-based method for soft and abrupt fault diagnosis of industrial gas turbines

Chen, Yu-Zhi; Zhang, Wei-Gang; Tsoutsanis, Elias; Zhao, Junjie; Tam, Ivan C. K. ...

2025-04-15
Elsevier
https://doi.org/10.1016/j.energy.2025.135358
Chen Y-Z, Zhang W-G, Tsoutsanis E, et al., (2025) An advanced performance-based method for soft and abrupt fault diagnosis of industrial gas turbines. Energy, Volume 321, April 2025, Article number 135358

Downloaded from a DSpace repository. https://dspace.org/